ACS ENGINEERING Au
AN OPEN ACCESS JOURNAL OF THE AMERICAN CHEMICAL SOCIETY

pubs.acs.org/engineeringau
Article

Chemical Aspect of Ocean Liming for CO_2 Removal: Dissolution Kinetics of Calcium Hydroxide in Seawater

Selene Varliero, Annamaria Buono, Stefano Caserini, Guido Raos,* and Piero Macchi*

Cite This: ACS Eng. Au 2024, 4, 422−431
Read Online

ACCESS | Metrics & More | Article Recommendations | Supporting Information

ABSTRACT: Ocean liming is attracting ever-increasing attention as one of the most suitable and convenient ways of removing carbon dioxide from the atmosphere and combating global warming and the acidification of the oceans at the same time. However, the short-term consequences of $Ca(OH)_2$ [slaked lime] dissolution in seawater have been scarcely studied. In this work, we investigate in detail what happens in the initial stages after the dissolution of slaked lime, analyzing the kinetics of the process and the effects on the physicochemical parameters of seawater. A series of experiments, carried out by varying the seawater conditions (like temperature and salinity) or the liming conditions (like the dispersion in the form of slurry or powder and the concentration) allow us to draw conclusions on the ideal conditions for a more efficient and environmentally friendly liming process.

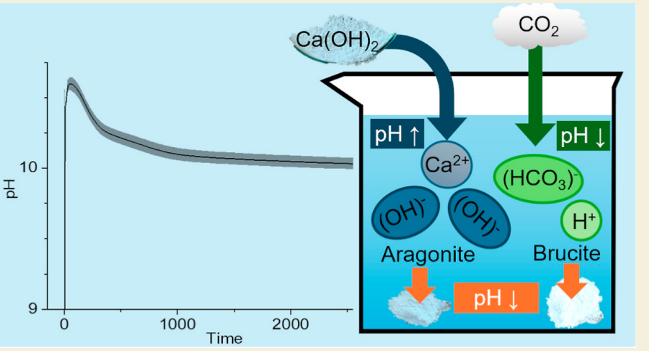

KEYWORDS: *CO_2 storage, climate change mitigation, marine chemistry, solution equilibria, enhanced weathering, carbonate system*

INTRODUCTION

Future scenarios that keep climate change well below 2 °C, following the commitment of the Paris Agreement, imply not only drastic reductions of greenhouse gas emissions but also the removal of hundreds of gigatons of carbon dioxide (CO_2) already present in the atmosphere.[1] In this context, there is considerable interest in methods that increase the alkalinity of the oceans to remove CO_2 from the atmosphere and simultaneously combat ocean acidification. According to the latest IPCC reports,[2,3] ocean alkalinity enhancement (OAE) is one of the ocean-based carbon dioxide removal methods that has a moderate to large future mitigation potential, despite its current limited deployment. Several authors have considered ocean liming (OL), i.e., the use of calcium hydroxide (also known as slaked lime, SL), for OAE.[4−6] SL is a relatively cheap material whose production could be upscaled to very large amounts, thanks to the wide availability of limestone.[7] It could be released, for example, in the wake of a ship, exploiting the turbulence created by the propellers to promote dissolution on the sea surface.[8]

The following chemical equation summarizes many aspects of the OAE process

$$Ca(OH)_{2(s)} + 2CO_{2(g)} \rightarrow Ca^{2+}_{(aq)} + 2HCO^{-}_{3(aq)} \quad (1)$$

First, since two moles of CO_2 are consumed by each mole of dissolved SL, the process is sustainable,[9] even considering that SL is obtained from calcium carbonate $CaCO_3$ and water, releasing one mole of CO_2 per mole of $Ca(OH)_2$. Second, the dissolution of SL implies the release of hydroxide anions and, hence, an increase in the seawater pH. This favors, in turn, the completion of reaction 1, with the conversion of carbon dioxide into bicarbonate ions.

Several authors studied the dissolution of SL in pure water and aqueous solutions. Some studies focused on the kinetics, measuring the dissolution of SL pellets in water[10] or in ionic solutions[11] by the rotating disc method. However, the kinetics of SL dissolution in seawater is yet to be investigated in detail, considering, in particular, its dispersion in the forms of powders or slurries with different concentrations. Concerning the salinity of the seawater, Sà and co-workers systematically studied the effects of SL dispersion in fresh, oligohaline, mesohaline, and euhaline water solutions in the context of aquaculture.[12,13] These authors pointed out that the addition of SL might reduce the alkalinity instead of increasing it due to the precipitation of $CaCO_3$ or $MgCO_3$ in carbonate-saturated waters

$$Ca^{2+}_{(aq)} + HCO^{-}_{3(aq)} + OH^{-}_{(aq)} \rightarrow CaCO_{3(s)} + H_2O_{(l)} \quad (2)$$

Received: February 29, 2024
Revised: April 27, 2024
Accepted: April 30, 2024
Published: May 15, 2024

The risk of "runaway precipitation" following OL with SL was also pointed out and analyzed more systematically in other studies,[14−16] focusing on the medium- and long-term effects on a time scale of several days. In those studies, the precipitation of other hydroxide minerals, such as brucite, is also suggested but not actually observed

$$Mg^{2+}_{(aq)} + 2OH^{-}_{(aq)} \rightarrow Mg(OH)_{2(s)} \quad (3)$$

The coprecipitation of other salts may also affect the rate of dissolution of SL, compared to the idealized conditions where this phenomenon does not occur.

A comprehensive model for the previous dissolution and precipitation reactions could be extremely useful in order to optimize OL operations, increasing the efficiency of CO_2 sequestration while minimizing the possible pitfalls and dangers for the marine environment. However, before further attempts toward quantitative modeling, it seems appropriate to collect more data under well-defined experimental conditions. Consequently, the aim of this work is to investigate the kinetics of SL dissolution in seawater, assessing the overall reaction rate under different conditions (temperature, salinity, etc.) and at different levels of SL concentration. In our experiments, we have added variable amounts of SL to natural and artificial seawater, both as powders and as slurries. The system was monitored by measuring changes in the solution pH and conductivity. Unlike previous studies,[12−16] we especially focus on short-term phenomena (minutes to hours), which are of great interest for assessing the potential side effects of SL dissolution. These include, for example, the impact of a spike in pH on the ecological functioning of the ocean, which may deserve future studies.

MATERIALS AND METHODS

Natural and Artificial Seawater

Artificial seawater was prepared by dissolving NaCl, Na_2SO_4, KCl, $MgCl_2{\cdot}6H_2O$, and $CaCl_2$ salts in purified water. All salts were Labkem products, purchased from Labbox, and used without further purification. We used the compositions proposed by Roy et al.[17] and detailed in Table S1 to obtain seawater with salinity S = 35. This is close to the average value of the Atlantic Ocean.[18] The same composition and ratios of salts were used to prepare seawater, with S = 10 and S = 40, representing the Baltic[19] and Mediterranean Sea,[20] respectively. Natural seawater was collected in March 2022 in Livorno, Italy (DD coordinates: 43.5299221, 10.3051620). It was then filtered with 0.2 μm sieves and shipped to our laboratory at Politecnico di Milano. The seawater was stored at 4 °C in a dark room in Nalgene tanks from the initial filtration to the last measurement, except for the 24 h transport, during which temperature could not be controlled.

Slaked Lime Preparation

Calcium hydroxide was generously provided by Unicalce S.p.A., featuring a purity of 93.96% and a median particle diameter of 9.2 μm. We tested the dissolution of two forms of SL, namely powder or slurry. The powder was directly poured into seawater without any premixing, under continuous stirring. The slurry was a 1.5 M suspension prepared by premixing with a spatula calcium hydroxide and the same seawater used for the experiments. After achieving a homogeneous dispersion (approximately 3 min of mixing), the mixture was poured into the seawater container.

General Experimental Procedures

SL was poured into beakers containing seawater solutions, in direct contact with the ambient atmosphere, and subjected to continuous stirring. During the dissolution experiments, we tested two types of agitation. Magnetic stirring was applied by using a magnetic bar sitting on the bottom of the beaker and rotating with an external magnetic field. Mechanical stirring was instead applied with a rotor inserted from the top of the solution, located at the center of the liquid column. In both cases, the chosen stirring rate (∼600 rpm) ensured good mixing but avoided turbulence or the formation of a vortex, which would have increased the area of the liquid−air interface. The temperature was maintained constant at the desired value with a LAUDA Eco Silver thermostatic bath. The pH, temperature, and conductivity (Λ) of the solution were continuously monitored with a Mettler Toledo Seven Excellence instrument calibrated on the NBS scale for pH. One hour after adding SL, the solutions were vacuum-filtered with a cutoff of 2−3 μm. The alkalinity of the solutions was measured ex situ by titration (Hanna Instruments HI84531) after filtration. The residues found after filtration were homogenized with a mortar and pestle and characterized by X-ray diffraction (XRD) using a Bruker D2-phaser powder diffractometer. Only a few grains of precipitated minerals were separated in the experiments with SL concentrations of 0.01 and 0.005 g/L. In this case, the material was too small to be homogenized with a mortar and pestle, so the few crystals were collected directly from the filter and analyzed with a Rigaku-Synergy-S single crystal X-ray diffractometer with a Gandolfi-type movement of the goniometer head.

SL Dosages

Most experiments on the effect of different SL dosages were carried out using artificial seawater and magnetic stirring. SL was in the form of a 1.5 M slurry. We divided the dissolution experiments into two SL dosage ranges: medium−high concentrations (0.4−8 g/L) and low concentrations (0.005−0.01 g/L). For the medium−high concentration, we used 1.5 L of artificial seawater, and each experiment was repeated three times. The low-concentration experiments were performed in a solution of 4.5 L of artificial seawater to increase the precision of the measured parameters. Each experiment with a low dosage was repeated two times. The low-concentration experiments were carried out without thermostatic control. In each experiment, the temperature was stable within 1 C, and the average temperatures of these experiments varied from 27 to 29 °C. See Table S2 in Supporting Information for more details.

Temperature and Salinity

Two sets of experiments were performed to assess the effects of temperature and salinity on SL dissolution. We used the same setup for medium−high concentration experiments: 1.5 L of artificial seawater, magnetic stirring, and SL as a 1.5 M slurry. To assess the effect of temperature on SL dissolution, we used artificial seawater at S = 35 and performed experiments with different temperatures, from 5 to 25 °C. To test the effect of salinity on SL dissolution, artificial seawater with salinities of 10, 35, and 40 was tested at 25 °C.

CO_2 Absorption

To monitor the carbon dioxide absorption, we used a 500 L box made of transparent poly(methylmetracrilate), sealed to avoid any exchange with the external atmosphere. We installed an atmospheric CO_2 sensor (ITSENSOR RCO2-W), pH sensor, and a conductivity sensor inside the box. The three parameters were automatically registered every 10 min. In addition, inside the box a fan with a diameter of 10 cm was activated to avoid air stratification. The initial CO_2 level was set to that of the external atmosphere without further control. Experiments were performed on 1.5 L of artificial (S = 35) or natural seawater mixed by magnetic stirring, and SL was delivered as a 1.5 M slurry. The box was closed just after the dispersion of SL and sealed for 40 h.

Theoretical Equilibrium Simulations

The likelihood of precipitation of a specific mineral phase may be linked to the saturation state of the solution, as measured by the saturation indexes Ω_X. For portlandite (the mineral form of SL), calcium carbonate (calcite CA, or aragonite AR) and brucite (BR), they are defined as follows

https://doi.org/10.1021/acsengineeringau.4c00008
ACS Eng. Au 2024, 4, 422−431

$$\Omega_{SL} = a(Ca^{2+})\cdot a(OH^-)^2/K_{sp}^{SL}$$
$$\Omega_{AR/CA} = a(Ca^{2+})\cdot a(CO_3^{2-})/K_{sp}^{AR/CA}$$
$$\Omega_{BR} = a(Mg^{2+})\cdot a(OH^-)^2/K_{sp}^{BR} \quad (4)$$

where K_{sp}^{X}'s are the thermodynamic constants for the dissolution equilibria (solubility products), and $a(i)$ is the activity of ion i, which depends on its concentration and the overall composition of the solution through the activity coefficient. The thermodynamic equilibria of artificial seawater with these mineral phases and atmospheric CO_2 were simulated with PHREEQC, a geochemical software developed by the US Geological Survey.[21] All calculations were performed using the "phreeqc.dat" database for the equilibrium constants and ion activities. For the sake of completeness, we investigated all of the minerals potentially involved in the process, not only those found as precipitated.

Table 1 summarizes how the different parameters have been measured or controlled.

Table 1. Summary of Parameters Analyzed and Equipment Used[a]

parameter	type	method/instrument
pH	M	potentiometry/Mettler Toledo seven excellence
conductivity	M	conductometry/Mettler Toledo seven excellence
temperature	C	thermostatic bath/LAUDA eco silver
atmospheric CO_2	M	CO_2 sensor in closed environment/ITSENSOR RCO2-W
precipitation	M	XRD/Bruker D2-phaser/Rigaku Synergy S
alkalinity	M	titration/Hanna Instruments HI84531
stirring	C	magnetic or mechanical stirrer
type of seawater	C	artificial or natural
salinity	C	salt concentration in artificial seawater
SL	C	different concentrations, in the form of powder or slurry

[a]The column type specifies whether the parameter has been controlled (C) or measured (M).

RESULTS AND DISCUSSION

Because of the complexity of SL dissolution in seawater and the subsequent uptake of atmospheric CO_2, a simultaneous exploration of all variables (temperature, salinity, type of seawater, concentration, initial form of SL, etc.) is extremely difficult. Therefore, we have designed a series of experiments to retrieve the qualitative (and possibly quantitative) effect of each variable, evaluated independently from the others. For this purpose, we have adopted a strategy summarized by the following workflow:

- Setting up the experiments with preliminary measurements.
- Selecting the ideal SL form and seawater conditions.
- Analyzing the dissolution of varying amounts of SL in artificial seawater at a fixed temperature (T = 25 °C) and salinity (S = 35).
- Assessing the effects of temperature and salinity.
- Comparing SL dissolution in natural and artificial seawater.
- Measuring the carbon dioxide absorption in seawater treated with SL.

Initial tests enabled a rapid screening of some experimental conditions, in particular the type of seawater, the form of the SL, and the stirring procedure. We tried, especially, to reduce random perturbations of the measurements that could affect the overall analysis. For example, artificial seawater is preferable in systematic studies because it guarantees higher reproducibility compared to natural seawater, which is instead subject to geographical and seasonal variations and requires filtering to remove larger particles and microorganisms, as well as special conservation at low temperatures in specific containers. We have therefore not considered all of the possible variables associated with natural seawater and used only one type for a general comparison against artificial seawater. We also point out that artificial seawater is often used in chemical studies concerning the behavior of carbonate minerals.[22,23] Similarly, the spreading of SL in the form of powder entails a slower and nonhomogeneous dissolution. In fact, some undissolved particles float on the surface while the remaining powder dissolves, inducing a high increase of pH, localized in the vicinity of the point of spreading, and consequent precipitation. Thus, the behavior of the powder is rather unpredictable and depends on more variables, like the particle size, the presence of contaminants, etc. There are also similar differences between the magnetic and mechanical stirring methods (see Figures S1 and S2 in the Supporting Information). Magnetic stirring was chosen for most experiments because it is less invasive than the mechanical one.

Temperature, salinity, and SL concentration are critical parameters that significantly affect the chemical equilibrium and the reaction kinetics of the carbonate system[24] and need to be carefully examined to establish the conditions for the most efficient seawater treatment. For these reasons, we investigated their effects with properly designed experiments.

We first investigated medium–high SL dosages, from 0.4 to 8 g/L. Figure 1 illustrates the consequent pH changes in artificial seawater of salinity S = 35 at T = 25 °C. The pH rises rapidly (within less than 1 min) to a value of about 10 for SL concentrations in the range of 0.4–2.0 g/L, while it rises to 10.5 for 4 g/L and to above 12 (in less than 30 s) for 8 g/L. These values agree with the numerical simulation, as discussed below. After reaching the climax, the pH decreases slowly and

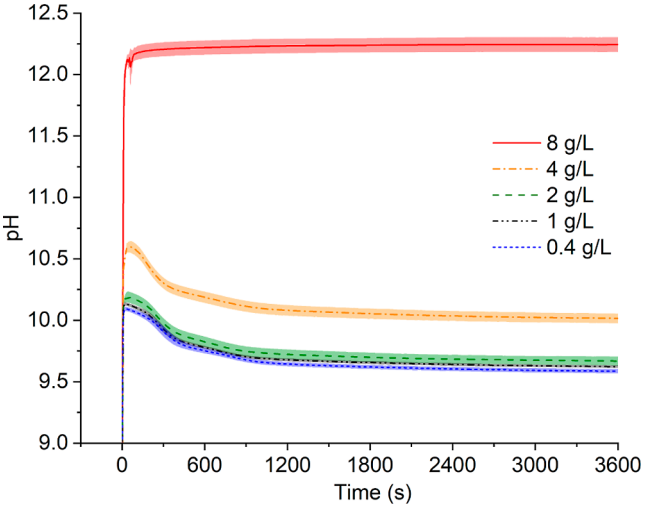

Figure 1. Measured pH following dissolution of a SL slurry (medium–high dosages) in artificial seawater (S = 35) at 25 °C. The quantities listed in the figure legend correspond to the equivalent amounts of dry SL powder. The error bar corresponds to the standard deviation of the interpolation curve. The initial pH was in the range of 6.6–7.2.

https://doi.org/10.1021/acsengineeringau.4c00008
ACS Eng. Au 2024, 4, 422–431

gradually, except for the largest SL dosage, for which a plateau is observed for the entire duration of the measurement. The origins of these differences are discussed below, in connection with the precipitation of mineral phases. The dissolution of SL also causes changes in the water conductivity (Figure S3). Since the conductivity of untreated seawater is already very high (about 50,000 μ S/cm at 25 °C), the changes are modest, typically less than 1%, except for the largest SL dosages. The addition of SL may cause a temporary dip in the seawater conductivity at times that roughly correspond to the maxima in the pH.

Mineral precipitation took place in all of these experiments. The precipitates were identified by XRD analysis of the powders collected after filtration. In the XRD diffractograms (Figures S4 and S5), we identified brucite [$Mg(OH)_2$], calcite and aragonite ($CaCO_3$), and halite (NaCl). No trace of undissolved calcium hydroxide in its crystalline form could be identified. Brucite is the dominant phase, with broad peaks which indicate small crystallites of $Mg(OH)_2$ compared to the other phases. This speaks for the rapid precipitation of $Mg(OH)_2$. Halite does not affect the process because crystals of NaCl likely form during the drying of the filtering paper, and it is therefore not a true precipitation (as in fact the solubility of NaCl in water is about 10 times larger than its concentration in seawater).

We then focused on low SL dosages. According to calculations performed with PHREEQC, an SL concentration lower than 0.01 g/L would produce $\Omega_{BR} \leq 0.85$, thus excluding precipitation of $Mg(OH)_2$. We have, therefore, tested the dispersion of 0.01 and 0.005 g/L of SL. Figure 2 reports the

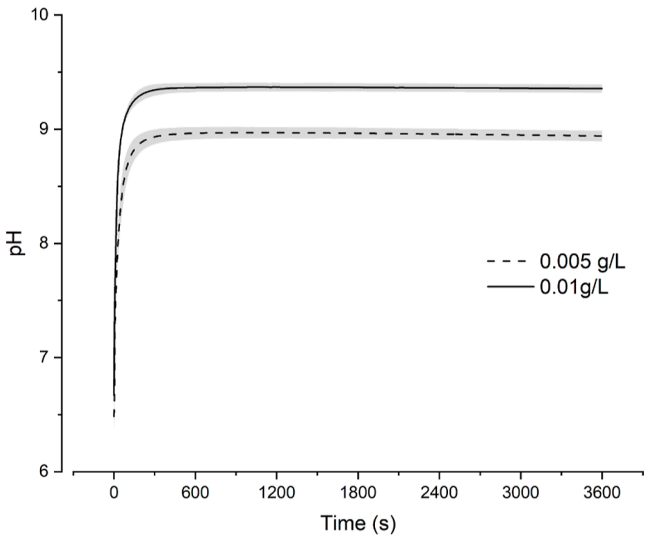

Figure 2. Measured pH following dissolution of a SL slurry (low dosages) in artificial seawater (S = 35) at room temperature. The quantities listed in the figure legend correspond to the equivalent amounts of dry SL powder. The error bar corresponds to the standard deviation of the interpolation curve. The initial pH was in the range of 6.5−7.1.

pH observed in artificial seawater after SL dissolution for these dosages. The pH reached plateaus of 9.38 and 8.97 for 0.01 and 0.005 g/L, respectively, without featuring any peak, as otherwise observed with higher dosages (Figure 1). Precipitation was much less abundant than after dosages of 0.4 g/L or higher. Only few crystals could be separated from the solutions. In these solids, we identified brucite and calcite for the 0.01 g/L dosages and only calcite for the 0.005 g/L experiments. The unexpected presence of brucite could be justified by its formation within the slurry and its incomplete dissolution afterward.

After testing the SL dosages at a fixed temperature and salinity, we analyzed the effects of changing these variables. Figure 3a reports the occurrence of pH peaks at various temperatures as a function of SL dissolution. It is evident that at lower T, a higher pH peak occurs. This agrees with the solubility of SL, which decreases at higher T.[25] Similarly, the SL dissolution is larger with a lower salinity of the seawater. As a consequence, for a SL concentration of 2 g/L, the pH maximum is attained at 12 in seawater with S = 10, whereas in seawater of higher salinity, the pH maximum is below 10.5 for the same concentration of SL [see Figure 3b].

We proceed with a comparison between natural and artificial seawater, although, as discussed above, natural seawater is extremely variable, and our comparison only refers to one particular sampling (see Materials and Methods for details). The pH of natural seawater is less sensitive to the addition of SL than that of artificial seawater; see, for example, the curves for medium SL dosages (0.4 to 2 g/L in Figure 4a), where the peak and long-time values of the pH of artificial seawater are higher than those of the natural one, even though the starting value of artificial seawater is about one pH unit lower. For 8 g/L, differences are instead negligible. Except for the higher concentration, for which the pH remains essentially constant over time, there is a noticeable decrease in pH within 1 h after the peak, see also Table 2. The time to reach the pH peak is comparable between the two types of solutions, but it is more difficult to locate it precisely in natural seawater because the pH features a broader maximum.

Figure 4b summarizes the behavior of natural and artificial seawater after SL addition in terms of pH_{max} and $\Delta\Lambda$. The latter is the difference between the conductivity of the untreated seawater and the one after the SL dosage (more precisely, the end point is calculated as the average value in the range from 50 to 60 min after the dosage to smooth out possible sudden spikes). For the SL concentrations of 0.4 and 1 g/L, natural and artificial seawater have almost negligible differences ($\Delta pH_{max} < 0.05$), which, however, are more noticeable (albeit still quite small) upon increasing the concentration. At the highest concentration of 8 g/L, though, one cannot distinguish the natural from the artificial seawater. A possible explanation for this behavior is given below, after the analysis of precipitated minerals.

The precipitates collected in both types of environments one h after the dissolution of 1 g/L of SL were analyzed with XRD (see Figure S4). In keeping with the discussion above, the main difference is that, in natural seawater, aragonite instead of brucite is the dominant crystal phase. This is likely explained by the different content of alkalinity and dissolved inorganic carbon (DIC), which are close to zero in our artificial seawater.[24] Instead, the presence of organic components (the so-called "dissolved organic matter" DOM) in natural seawater has an inhibitory effect on $CaCO_3$ precipitation. The DOM is naturally present in seawater in the range of 50−70 μM, depending on the type of sea and on the season.[26] Moreover, the DIC endows natural seawater with a certain buffering power, which explains the differences of pH behavior shown in Figure 4 and Table 2. The higher pH peaks of artificial seawater and the plateau of natural seawater illustrate the

https://doi.org/10.1021/acsengineeringau.4c00008
ACS Eng. Au 2024, 4, 422−431

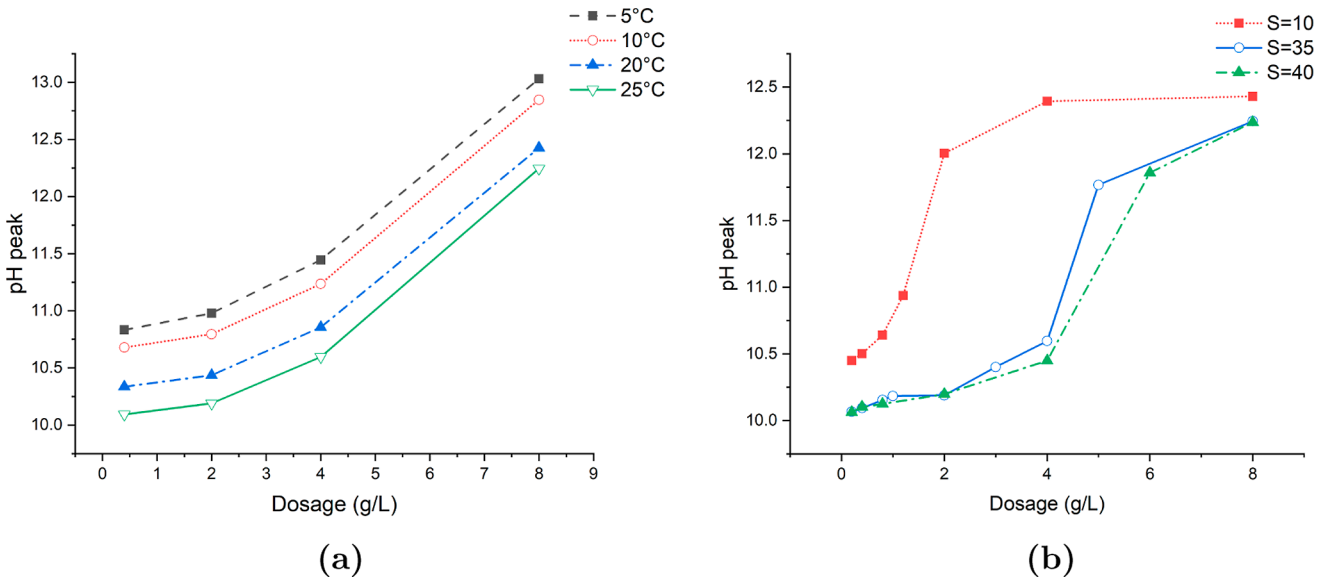

Figure 3. Variation of maximum pH as a function of temperature and salinity, following the dissolution of SL in artificial seawater. (a) Effect of temperature at S = 35. (b) Effect of the salinity at T = 25 °C.

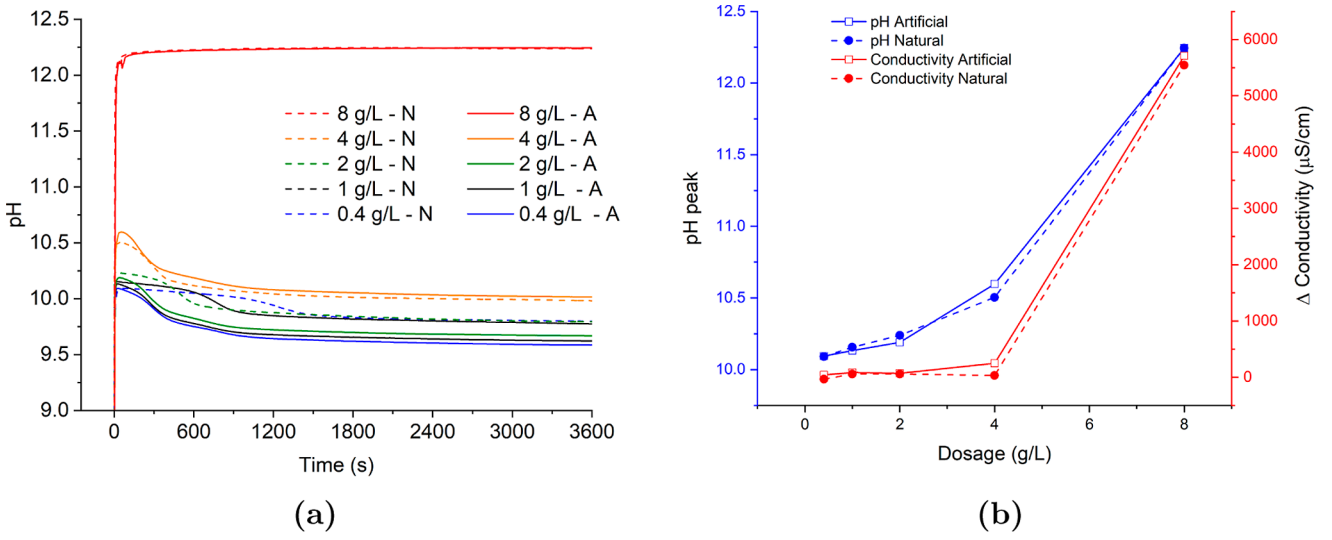

Figure 4. (a) Effect of SL slurry dosage on the pH, following dissolution in natural (N) and artificial (A) seawater. The initial pH range is between 6.6 and 7.2 for artificial seawater, and it is between 7.9 and 8.1 for natural seawater. (b) Summary of the SL dissolution experiments from 0.4 to 8 g/L, in artificial and natural seawater at T = 25 °C.

Table 2. pH Change from the Climax (Occurring Few Minutes after the SL Addition) to the Stabilization after 60 min in Natural and Artificial Seawater at T = 25 °C

	ΔpH	
dosage (g/L)	artificial seawater	natural seawater
0.4	−0.51	−0.29
1	−0.51	−0.38
2	−0.52	−0.45
4	−0.58	−0.52
8	−0.001	−0.007

different resistance to pH variation, which is larger for the natural seawater thanks to the buffering capacity of a more alkaline solution. At 8 g/L, the buffering power is, however, exhausted and no significant difference is observable between natural and artificial seawater. Apart from the pH, natural seawater differs from the artificial one because, after the SL treatment: (a) the alkalinity does not increase but mildly decreases; (b) there is significantly less brucite in the precipitate, whereas aragonite appears, together with calcite. These two features are somewhat connected. In natural seawater, the tested SL dosages (≥0.05 g/L) reduces the alkalinity because of the carbonate (aragonite and calcite) precipitation (see Figure 5).[12−14] Therefore, the precipitation of carbonate minerals reduces the efficiency of the alkalinization process and the storage capacity of CO_2, as explained later in the paper. Note that aragonite is thermodynamically less stable than calcite, but it forms preferentially because magnesium has an inhibitory effect on calcite precipitation.[27] On the other hand, the absence of carbonate ions in artificial seawater implies that the initial alkalinity is negligible below the instrument's detection limit (600 μM), and therefore, it increases upon SL addition.

https://doi.org/10.1021/acsengineeringau.4c00008
ACS Eng. Au 2024, 4, 422−431

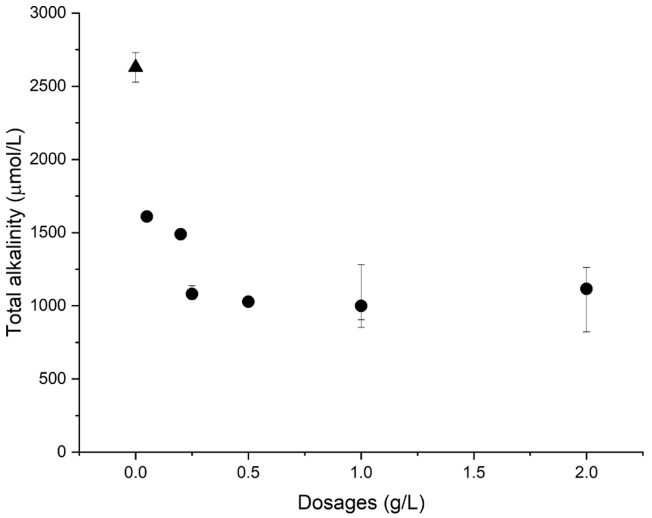

Figure 5. Effect of SL slurry dosage on the total alkalinity, following dissolution in natural seawater. The symbol and error bar at zero dosage refer to untreated natural seawater.

We now focus on CO_2 absorption. Figure 6 shows that CO_2 concentration decreases almost linearly from the atmosphere above the seawater solution, at least when the starting point is above 400 ppm (noteworthy, the average atmospheric concentration as of 2023 is about 420 ppm).[28] The opposite of the time derivative of the fitted functions (Table 3) indicates the rate of the carbon dioxide absorption in the solution. Given that the gas−liquid interface area is identical for all of the experiments, we can neglect this geometrical effect on the absorption. The rate grows with the SL dosage, although not linearly, and one may anticipate that for dosages larger than 1 g/L the rate would approximately stabilize at ca. 1.5 ppm/h. The difference between artificial and natural seawater is small and likely within the uncertainties of the measuring method. On the other hand, Figure 6 shows clearly that CO_2 is absorbed more rapidly in pure water, and therefore one can anticipate that the absorption would be more efficient in seawater of lower salinity. Table 4 reports the theoretical ($\Delta CO_{2,th}$) and experimental ($\Delta CO_{2,exp}$) reduction of CO_2 in atmosphere, expressed in mmol. Natural seawater seems to absorb more carbon dioxide than artificial seawater, but as for the absorption rate in Table 3, the statistic is not strong enough to allow for conclusions. Indeed, it is clear that all of the experiments do not reach the expected CO_2 absorption due to two main factors. At 40 h, the solution is not yet equilibrated with the air (see Figure 6); moreover, as discussed below, the precipitation of brucite, aragonite, and calcite lowers the maximum amount of CO_2 that the solution can absorb.

Figure 7 reports the theoretical solubility limits of calcite, aragonite, and brucite in pure water and in artificial seawater at

Table 3. Absorption Rates Calculated from the Linear Regression of CO_2 vs t in the Atmosphere Above the Solution for Various Dosages and Seawater Types

	$-d[CO_2]/dt$ (ppm/h)	
$Ca(OH)_2$ (g/L)	artificial	natural
0.25	0.86	0.66
0.50	1.34	1.32
1.00	1.37	1.56

Table 4. Potential and Effective Decrease of Carbon Dioxide in the Atmosphere According to the Kind of Seawater and SL Dosages[a]

		$\Delta CO_{2,exp}$ (mmol)	
$Ca(OH)_2$ (g/L)	$\Delta CO_{2,th}$ (mmol)	artificial	natural
0.25	10.12	0.45	0.47
0.50	20.25	0.65	0.78
1.00	40.49	0.69	0.86

[a]$\Delta CO_{2,th}$ reports the expected CO_2 reduction according to stoichiometry, and $\Delta CO_{2,exp}$ shows the effective decrease in the atmosphere.

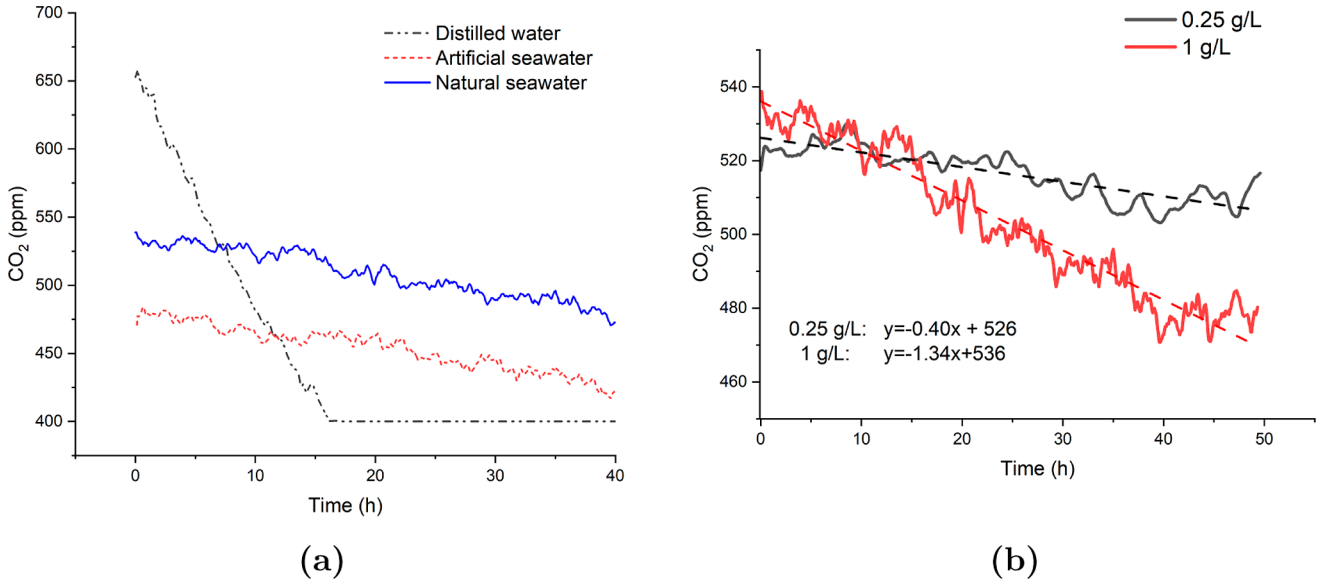

Figure 6. Gaseous CO_2 concentration within a closed chamber containing SL-treated solutions. The data are represented as running averages over windows of 15 min. (a) Effect of water type on a 1 g/L dosage. The plateau at 400 ppm in the plot for distilled water corresponds to the lowest detection limit of the CO_2 sensor. (b) Effect of the SL dosage on natural seawater.

https://doi.org/10.1021/acsengineeringau.4c00008
ACS Eng. Au 2024, 4, 422−431

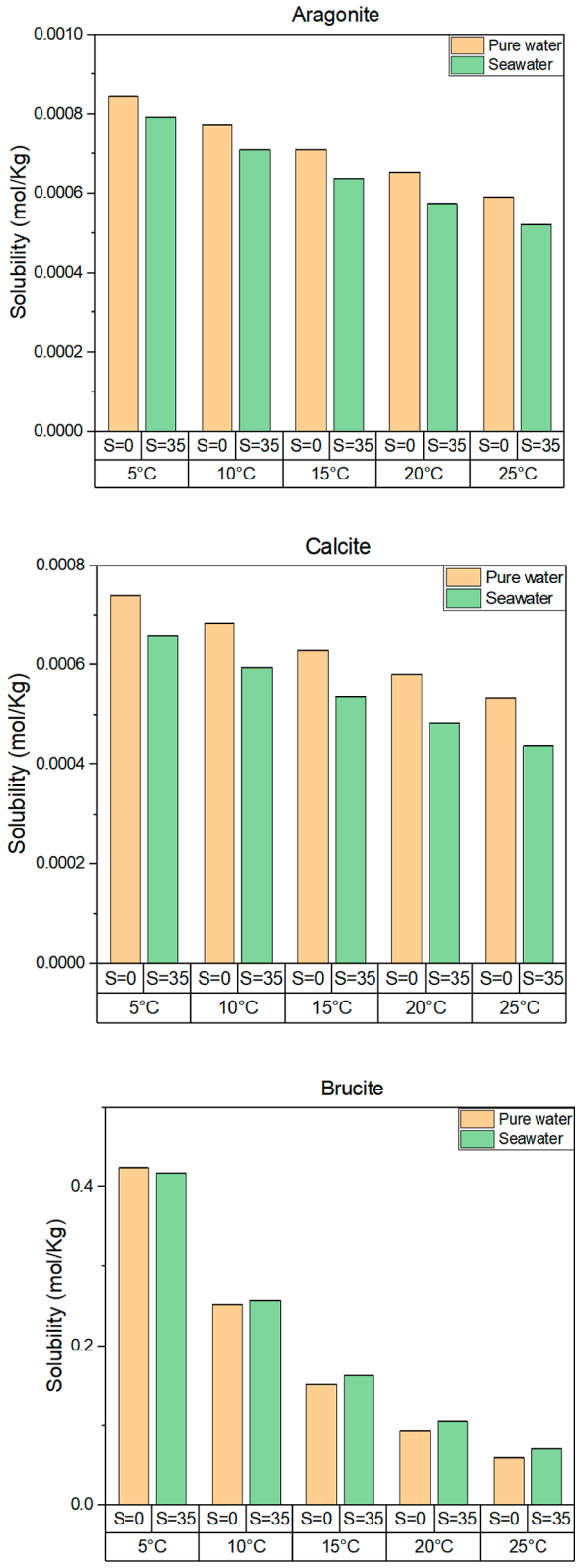

Figure 7. PHREEQC calculation of mineral solubility (mol/kg) in pure water ($S = 0$) and artificial seawater ($S = 35$) in equilibrium with an atmosphere containing 400 ppm of CO_2. See Tables S3 and S4 in Supporting Information for the numerical values.

different temperatures, calculated with PHREEQC. Calcite and aragonite are expected to have a very low solubility, which further decreases with the increase of salinity or temperature. The theoretical solubilities of brucite, instead, increase slightly with salinity, while they decrease with temperature. PHREEQC also allows a calculation of the pH of artificial seawater and the amount and type of precipitate after dissolving SL. The simulations consider a solution at equilibrium with all the relevant minerals phases: calcite, aragonite, brucite, and portlandite. As for the equilibrium with the atmosphere, the model considers only the equilibrium with the CO_2 of the initial solution but not after the SL dissolution. This approximation is acceptable because the absorption of atmospheric CO_2 by the solution is much slower (occurring on a time scale of days, in keeping with the absorption rates reported above). So, the atmospheric CO_2 concentration should not significantly affect the precipitates analyzed 1 h after SL dissolution.

Figure 8 reports the calculated amounts of precipitate of each mineral according to the simulation. The model predicts a complete precipitation of brucite after dissolving 4 g/L of SL and a partial precipitation of portlandite after addition of 5 g/L of SL. These two curves affect the pH, which drastically increases after the brucite total precipitation because there is no longer a sink for the $(OH)^-$ ions, but it stabilizes after reaching the solubility point of calcium hydroxide because there is no longer a source of $(OH)^-$. The precipitation of calcite seamlessly follows the pH, although the solid form grows in much lower quantity compared to brucite (about 3 orders of magnitude). According to PHREEQC, in artificial seawater, the SL reaches saturation at about 5.15 g/L, although we have not found undissolved SL even after the addition of 8 g/L SL. This suggests that the simulation performed with PHREEQC should require refinement to achieve a complete description of the system, especially close to the SL saturation point. The lack of portlandite in the XRD data may also be explained by the precipitation of a small amount of amorphous calcium hydroxide.

We then simulated the thermodynamic equilibrium between the artificial seawater, initially in equilibrium with atmospheric carbon dioxide and only the mineral phases observed experimentally, namely calcite, aragonite, and brucite. Table 5 reports the pH calculated for models constrained to (a) no precipitation; (b) precipitation of calcite and aragonite only; (c) precipitation of brucite only; (d) all three species simultaneously precipitate. For the sake of comparison, we also report the pH measured experimentally 10 min after the SL dosage. According to the pH trend (Figure 1), the precipitation phenomena are almost finished, and the CO_2 absorption has not yet affected the solution. The model including the brucite precipitation is definitely closer to the experiment, with differences below 0.3, except for the SL dosage of 4 g/L. At an 8 g/L dosage, the difference between the two models is almost negligible because SL dissolution dominates over any kind of precipitation.

Medium and high dosages of slacked lime entail the precipitation of both calcium carbonate morphologies (aragonite and calcite) and magnesium hydroxide (brucite), whereas this is smaller for lower SL dosages. Because the brucite precipitation directly subtracts hydroxide ions from the solution [see reaction 3], the pH is directly affected. However, this is particularly cogent for dosages up to 4 g/L. Above this value, in facts, the simulations indicate that the brucite precipitation is almost exhausted [see Figure 8a] and can no longer influence the pH. Therefore, for medium dosages, after a rapid increase, the pH also rapidly decreases due to the $(OH)^-$ consumption, thus producing the observed peak that is

https://doi.org/10.1021/acsengineeringau.4c00008
ACS Eng. Au 2024, 4, 422−431

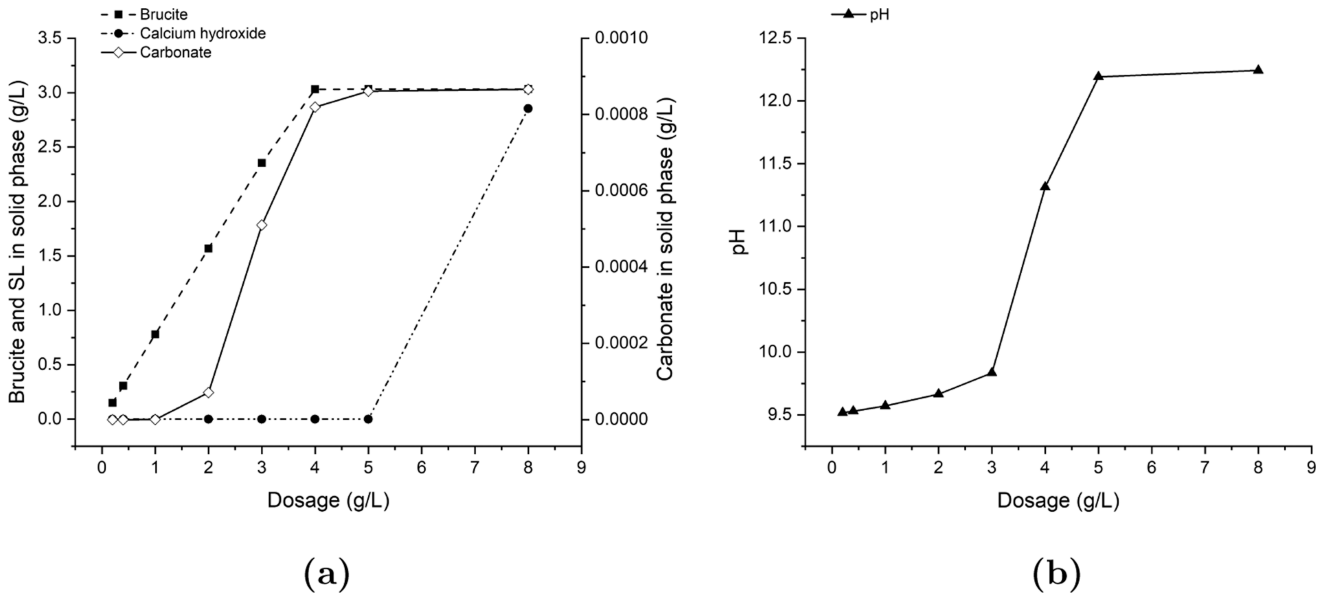

Figure 8. Theoretical amount of mineral precipitation (a) and pH (b) after the dissolution of SL in artificial seawater with S = 35 at T = 25 °C.

Table 5. pH Calculated for Various SL Dosages with Models Excluding (a and b) or Including (c and d) the Precipitation of Brucite[a]

SL dosage (g/L)	model (a) and (b)	model (c) and (d)	expt.
0.005	9.13	9.13	8.67
0.01	9.47	9.47	9.36
0.4	11.18	9.53	9.75
1	11.66	9.57	9.78
2	12.09	9.67	9.82
4	12.35	11.31	10.19
8	12.35	12.24	12.22

[a]Experimental values, measured 10 min after each dosage, are also reported.

observed. For higher dosage, instead, the brucite precipitation does not subtract enough $(OH)^-$ and the pH remains high. The precipitation of carbonate minerals, instead, removes bicarbonate ions [reaction 2], directly affecting the alkalinity. From the XRD diffractograms, the peaks associated with brucite are much broader than those of the carbonate minerals. This indicates the small size of the brucite crystallites. The peak intensities also reveal the abundance of this species. Therefore, brucite undergoes massive and fast precipitation. From these results, we can also infer that the whole SL dissolves and reacts with seawater, excluding the formation of a sort of "protective coating" of the SL particles through the precipitation of less soluble phases. The strong and relevant contribution of brucite precipitation to pH is consistent with the better agreement of models (c) and (d), compared with models (a) and (b), with experimental values, as reported in Table 5. The most significant discrepancy between models (c) and (d) and the experimentally measured pH occurs for SL concentration of 4 g/L. Again, this may be due to the SL concentration being close to the saturation point of brucite: a situation more difficult to model because extremely sensitive to even small fluctuations. At 8 g/L dosage, the difference among the cases is lower, pointing out that after brucite saturation the pH is less affected by precipitation. The precipitation of minerals also explains the behavior of conductivity. In particular, a temporary dip in conductivity was observed right after SL introduction, in correspondence with the pH peak. Since the peak of pH is associated with the fast precipitation of mineral phases, there is also a subtraction of ions from the solution that reduces the conductivity.

The absorption of CO_2 from the atmosphere contributes to pH reduction. However, while precipitation of minerals is a rapid phenomenon occurring on the time scale of minutes (if not seconds), CO_2 absorption is much slower and requires hours. Therefore, the pH decrease due to absorption is visible only much later than the effects of mineral precipitation.

A final remark concerns the application of OL. Of course, any kind of seawater can be used to capture carbon dioxide from the atmosphere, a process that is in principle facilitated by a higher amount of SL discharge. However, the excessive pH that can be reached with high SL dosages and the induced mineral precipitation are important side effects that abruptly modify the overall efficiency of the process. As is easily conceivable, a very high pH, even if reached for only a few seconds, may significantly affect the living organisms in seawater (the so-called marine biota). A recent study assessed that for pH equal to 9, copepods do not suffer side effects in 6 h.[29] So, pH 9 can be used as threshold for a safe application.

Apart from the pH, mineral precipitation is also quite relevant. Formation of brucite reduces the efficiency of SL dissolution because consuming directly the $(OH)^-$ ions, which is an obvious short-circuit. Moreover, carbonate precipitation also has a negative effect because it acts against the alkalinity and reduces the seawater buffering capacity. As a matter of fact, the efficiency of the process will be lower if $CaCO_3$ precipitates because the desired increase of alkalinity will not be reached and CO_2 will be released during $CaCO_3$ formation.

Table 6 summarizes how different seawater conditions affect the pH and carbonate precipitation. As shown in Figure 3, after SL dissolution, the pH increases less if the temperature and the salinity are higher. This agrees with the PHREEQC simulation (see Figure 7), which shows that the solubility of calcite and aragonite also decreases as the temperature and salinity increase,[30,31] while brucite solubility decreases with temper-

https://doi.org/10.1021/acsengineeringau.4c00008
ACS Eng. Au 2024, 4, 422−431

Table 6. Summary of How the Different Parameters Influences SL Dissolution[a]

parameters		effects
salinity ↑		pH ↓—$CaCO_3$ precipitation ↑
temperature ↑		pH ↓—$CaCO_3$ precipitation ↑
SL concentration ↑	⇒	pH ↑—$CaCO_3$ precipitation ↑
slurry form of SL		homogeneity ↑

[a]The arrows indicate how the pH reacts to the variation of one parameter. The symbol ↑ means "increase" and ↓ means "decrease". E.g., a salinity increase will entail an increase in carbonate precipitation and a pH decrease.

ature but increases with salinity. Therefore, cold and less salty seas, such as the Baltic Sea, will be preferable for the most efficient SL treatment. In contrast, in seas such as the Mediterranean, where the precipitation is facilitated, the dosage of SL should be kept lower, thus reducing the overall OL benefits. In general, the lower dosages of SL are those that maximize the efficiency (i.e., CO_2 absorption per quantity of dissolved SL) with lowest impact on the seawater physical and chemical parameters hence on the marine biota.

CONCLUSIONS

OL by dispersion of SL is a process that attracts ever-growing attention as a way of capturing CO_2 from the atmosphere and limiting ocean acidification. We have here reported a thorough study of seawater modifications upon the discharge of slaked lime, aimed at monitoring the initial instants after the SL discharge, when the dissolution process has not reached equilibrium yet and many parameters, like pH, may be severely affected. The knowledge and control of these chemical variables are fundamental for a properly conducted, safe, and efficient application of OL. For this purpose, it is important to identify the largest amount of SL that could be dissolved, e.g., discharging in the wake of a ship, without producing pH spikes that could be dangerous for marine life and avoiding carbonate precipitation.

We have been able to identify:

- the ideal SL dosage: ≤0.005 g/L;
- the ideal seawater conditions: low temperature and salinity, as in Baltic sea;
- the most efficient SL form: predissolved SL, as slurry;
- possible unwanted side reactions: brucite, aragonite, and calcite precipitation.

A safe threshold for the SL dosage is approximately 0.005 g/L, which is the lowest concentration we tested. Strong and rapid dilution of SL could significantly increase this limit, if necessary. A more precise assessment would, however, require modeling the fluid dynamics of the discharge and the kinetics of the SL dissolution. As for the seawater conditions, dissolution is faster at low temperatures and low salinity, which also slows down the precipitation of other minerals (brucite, calcite, and aragonite). The slurry is the most advisable SL form because it results in more homogeneous conditions and predictable behavior, whereas dispersion in the form of powder entails higher localized and dangerous concentration of SL. In this work, we also provided a simple demonstrative test of the efficiency of OL by measuring the decrease of CO_2 in the atmosphere of an isolated system in which seawater received a SL treatment. We hope that all of these results could be of interest to scientists and engineers working on the optimization of ocean alkalinization through SL.

ASSOCIATED CONTENT

Supporting Information

The Supporting Information is available free of charge at https://pubs.acs.org/doi/10.1021/acsengineeringau.4c00008.

Chemical composition of artificial seawater at different salinities; temperature variation in low-dosage experiments, performed without temperature control; effect of the physical state of SL (powder or slurry) on the pH during dissolution in artificial seawater, with S = 35 at T = 25 °C; effect of the stirring mode on the measured pH during dissolution of SL slurry in artificial seawater, with S = 35 at T = 25 °C; conductivity variation from the initial value (before SL addition) during dissolution experiments of SL slurry (1.5 M) in artificial (S = 35) seawater at T = 25 °C; XRD pattern and peak assignment for filtered matter following 1 h dissolution of SL in natural and artificial seawater; XRD pattern and peak assignment for filtered matter following 1 h dissolution of 8 g/L SL in artificial seawater; PHREEQC calculation of mineral solubility in artificial seawater (S = 35) in equilibrium with an atmosphere containing 400 ppm of CO_2; and PHREEQC calculation of mineral solubility in pure water in equilibrium with an atmosphere containing 400 ppm of CO_2 (PDF)

AUTHOR INFORMATION

Corresponding Authors

Guido Raos − *Department of Chemistry, Materials and Chemical Engineering "G. Natta", Politecnico di Milano, Milano I-20131, Italy; CoNISMa—Consorzio Nazionale Interuniversitario per le Scienze del Mare, Roma 00196, Italy;* orcid.org/0000-0001-7011-4036; Email: guido.raos@polimi.it

Piero Macchi − *Department of Chemistry, Materials and Chemical Engineering "G. Natta", Politecnico di Milano, Milano I-20131, Italy;* orcid.org/0000-0001-6292-9825; Email: piero.macchi@polimi.it

Authors

Selene Varliero − *Department of Chemistry, Materials and Chemical Engineering "G. Natta", Politecnico di Milano, Milano I-20131, Italy*

Annamaria Buono − *Department of Chemistry, Materials and Chemical Engineering "G. Natta", Politecnico di Milano, Milano I-20131, Italy*

Stefano Caserini − *Department Engineering and Architecture, University of Parma, Parma 43124, Italy;* orcid.org/0000-0002-7937-9206

Complete contact information is available at: https://pubs.acs.org/10.1021/acsengineeringau.4c00008

Author Contributions

CRediT: **Selene Varliero** conceptualization, data curation, formal analysis, methodology, writing-original draft, writing-review & editing; **Annamaria Buono** data curation, formal analysis, writing-review & editing; **Stefano Caserini** conceptualization, funding acquisition, writing-review & editing; **Guido Raos** conceptualization, formal analysis, funding acquisition,

https://doi.org/10.1021/acsengineeringau.4c00008
ACS Eng. Au 2024, 4, 422−431

investigation, methodology, project administration, resources, supervision, writing-original draft, writing-review & editing; **Piero Macchi** conceptualization, data curation, formal analysis, funding acquisition, investigation, methodology, project administration, resources, supervision, writing-original draft, writing-review & editing.

Notes

The authors declare no competing financial interest.

■ ACKNOWLEDGMENTS

The authors thank Francesco Crisanto and Matteo Colombo for their precious collaboration in the set-up and a series of preliminary experiments. The European Lime Association (EuLA) is thanked for financial support through a contract with CoNISMa.

■ REFERENCES

(1) IPCC, 2019: Summary for Policymakers Pörtner, H.-O.; Roberts, D. C.; Masson-Delmotte, V.; Zhai, P.; Tignor, M.; Poloczanska, E.; Mintenbeck, K.; Alegría, A.; Nicolai, M.; Okem, A.; Petzold, J.; Rama, B.; Weyer, N. M. *Special Report on the Ocean and Cryosphere in a Changing Climate*; IPCC, 2019.

(2) Cross-sectoral perspectives Babiker, M.; Berndes, G.; Blok, K.; Cowie, A.; Geden, O.; Ginzburg, V.; Leip, A.; Smith, P.; Sugiyama, M.; Yamba, F. *Climate Change 2022: Mitigation of Climate Change. Contribution of Working Group III to the Sixth Assessment Report of the Intergovernmental Panel on Climate Change 2022, Table 12.5*; IPCC, 2022.

(3) Pathak, M.; Slade, R.; Pichs-Madruga, R.; Ürge-Vorsatz, D.; Shukla, R.; Skea, J. *Climate Change 2022 Mitigation of Climate Change; Technical Summary*, 2022. Chapter TS.5.7.

(4) Renforth, P.; Kruger, T. Coupling mineral carbonation and ocean liming. *Energy Fuels* **2013**, *27*, 4199−4207.

(5) Renforth, P.; Henderson, G. Assessing ocean alkalinity for carbon sequestration. *Rev. Geophys.* **2017**, *55*, 636−674.

(6) Caserini, S.; Barreto, B.; Lanfredi, C.; Cappello, G.; Ross Morrey, D.; Grosso, M. Affordable CO_2 negative emission through hydrogen from biomass, ocean liming, and CO_2 storage. *Mitig. Adapt. Strateg. Glob. Chang.* **2019**, *24*, 1231−1248.

(7) Caserini, S.; Storni, N.; Grosso, M. The availability of limestone and other raw materials for ocean alkalinity enhancement. *Global Biogeochem. Cycles* **2022**, *36*, No. e2021GB007246.

(8) Caserini, S.; Pagano, D.; Campo, F.; Abbà, A.; De Marco, S.; Righi, D.; Renforth, P.; Grosso, M. Potential of maritime transport for ocean liming and atmospheric CO_2 removal. *Front. Clim.* **2021**, *3*, 575900.

(9) Foteinis, S.; Andresen, J.; Campo, F.; Caserini, S.; Renforth, P. Life cycle assessment of ocean liming for carbon dioxide removal from the atmosphere. *J. Cleaner Prod.* **2022**, *370*, 133309.

(10) Wang, J.; Keener, T. C.; Li, G.; Khang, S.-J. The dissolution rate of $Ca(OH)_2$ in aqueous solutions. *Chem. Eng. Commun.* **1998**, *169*, 167−184.

(11) Giles, D.; Ritchie, I.; Xu, B.-A. The kinetics of dissolution of slaked lime. *Hydrometallurgy* **1993**, *32*, 119−128.

(12) Sá, M. V.; Boyd, C. E. Dissolution rate of calcium carbonate and calcium hydroxide in saline waters and its relevance for aquaculture. *Aquaculture* **2017**, *469*, 102−105.

(13) e Sá, M. V. d. C.; Cavalcante, D.; Lima, F. R. d. S. Dissolution rates of hydrated lime, $Ca(OH)_2$ in fresh, oligohaline, mesohaline and euhaline waters and its significance for liming of shrimp culture ponds. *Aquacult. Res.* **2019**, *50*, 1618−1625.

(14) Moras, C. A.; Bach, L. T.; Cyronak, T.; Joannes-Boyau, R.; Schulz, K. G. Ocean alkalinity enhancement−avoiding runaway $CaCO_3$ precipitation during quick and hydrated lime dissolution. *Biogeosciences* **2022**, *19*, 3537−3557.

(15) Hartmann, J.; Suitner, N.; Lim, C.; Schneider, J.; Marín-Samper, L.; Arístegui, J.; Renforth, P.; Taucher, J.; Riebesell, U. Stability of alkalinity in ocean alkalinity enhancement (OAE) approaches−consequences for durability of CO_2 storage. *Biogeosciences Discuss.* **2023**, *20*, 781−802.

(16) Suitner, N.; Faucher, G.; Lim, C.; Schneider, J.; Moras, C. A.; Riebesell, U.; Hartmann, J. *Ocean Alkalinity Enhancement Approaches and the Predictability of Runaway Precipitation Processes−Results of an Experimental Study to Determine Critical Alkalinity Ranges for Safe and Sustainable Application Scenarios*; EGUsphere, 2023.

(17) Roy, R. N.; Roy, L. N.; Vogel, K. M.; Porter-Moore, C.; Pearson, T.; Good, C. E.; Millero, F. J.; Campbell, D. M. The dissociation constants of carbonic acid in seawater at salinities 5 to 45 and temperatures 0 to 45°C. *Mar. Chem.* **1993**, *44*, 249−267.

(18) Reverdin, G.; Kestenare, E.; Frankignoul, C.; Delcroix, T. Surface salinity in the Atlantic Ocean (30°S−50°N). *Prog. Oceanogr.* **2007**, *73*, 311−340.

(19) Janssen, F.; Schrum, C.; Backhaus, J. A climatological dataset of temperature and salinity for the North Sea and the Baltic Sea. *Dtsch. Hydrogr. Z.* **1999**, *51*, S.

(20) Brasseur, P.; Beckers, J.-M.; Brankart, J.; Schoenauen, R. Seasonal temperature and salinity fields in the Mediterranean Sea: Climatological analyses of a historical data set. *Deep Sea Res., Part I* **1996**, *43*, 159−192.

(21) Parkhurst, D. L.; Appelo, C. *Description of Input and Examples for Phreeqc Version 3—A Computer Program For Speciation, Batch-Reaction, One-Dimensional Transport, And Inverse Geochemical Calculations*; US Geological Survey Techniques And Methods, 2013; Vol. 6, p 497.

(22) Zuddas, P.; Mucci, A. Kinetics of calcite precipitation from seawater: II. The influence of the ionic strength. *Geochim. Cosmochim. Acta* **1998**, *62*, 757−766.

(23) Zhong, S.; Mucci, A. Calcite and aragonite precipitation from seawater solutions of various salinities: Precipitation rates and overgrowth compositions. *Chem. Geol.* **1989**, *78*, 283−299.

(24) Zeebe, R. E.; Wolf-Gladrow, D. *CO_2 in Seawater: Equilibrium, Kinetics, Isotopes*; Gulf Professional Publishing, 2001.

(25) Miller, L.; Witt, J. Solubility of calcium hydroxide. *J. Phys. Chem.* **1929**, *33*, 285−289.

(26) Hansell, D. A.; Carlson, C. A. *Biogeochemistry of Marine Dissolved Organic Matter*; Academic Press, 2014.

(27) Zhang, Z.; Xie, Y.; Xu, X.; Pan, H.; Tang, R. Transformation of amorphous calcium carbonate into aragonite. *J. Cryst. Growth* **2012**, *343*, 62−67.

(28) https://gml.noaa.gov/ccgg/trends/ (accessed 02, 2024).

(29) Camatti, E.; Valsecchi, S.; Caserini, S.; Barbaccia, E.; Santinelli, C.; Basso, D.; Azzellino, A. Short-term impact assessment of ocean liming: A copepod exposure test. *Mar. Pollut. Bull.* **2024**, *198*, 115833.

(30) McGee, K. A.; Hostetler, P. B. Activity-product constants of brucite from 10° to 90°C. *J. Res. US Geol Surv* **1977**, *5*, 227−233.

(31) Mucci, A. The solubility of calcite and aragonite in seawater at various salinities, temperatures, and one atmosphere total pressure. *Am. J. Sci.* **1983**, *283*, 780−799.

https://doi.org/10.1021/acsengineeringau.4c00008
ACS Eng. Au 2024, 4, 422−431